

Portland State University

PDXScholar

Civil and Environmental Engineering Faculty
Publications and Presentations

Civil and Environmental Engineering

6-2024

Advanced Acoustic Emission-based SHM for Concrete Structures: Real-Time, High-Precision Imaging of Crack Geometry and Damage Sourcetype Using Moment Tensor Inversion

Seyyedmaalek Momeni
EPFL, Geo-Energy Lab

Thomas Schumacher
Portland State University, thomas.schumacher@pdx.edu

Lindsay Linzer
SRK Consulting Ltd

Brice Lecampion
EPFL, Geo-Energy Lab

Follow this and additional works at: https://pdxscholar.library.pdx.edu/cengin_fac



Part of the [Civil and Environmental Engineering Commons](#)

Let us know how access to this document benefits you.

Citation Details

Momeni, Seyyedmaalek; Schumacher, Thomas; Linzer, Lindsay and Lecampion, Brice "Advanced Acoustic Emission-based SHM for Concrete Structures: Real-Time, High-Precision Imaging of Crack Geometry and Damage Sourcetype Using Moment Tensor Inversion" 1th European Workshop on Structural Health Monitoring (EWSHM 2024).

This Article is brought to you for free and open access. It has been accepted for inclusion in Civil and Environmental Engineering Faculty Publications and Presentations by an authorized administrator of PDXScholar. Please contact us if we can make this document more accessible: pdxscholar@pdx.edu.

Advanced Acoustic Emission-based SHM for Concrete Structures: Real-Time, High-Precision Imaging of Crack Geometry and Damage Source-type Using Moment Tensor Inversion

Seyyedmaalek MOMENI 1, Thomas SCHUMACHER 2, Lindsay LINZER 3, Brice LECAMPION 1

1 EPFL, Geo-Energy Lab, Lausanne, Switzerland, seyyedmaalek.momeni@epfl.ch,
2 Civil and Environmental Engineering, Portland State University, Portland, USA,

3 SRK Consulting Ltd, Johannesburg, South Africa

Abstract. In this paper, we introduce a novel automated and high-precision acoustic emission (AE) monitoring algorithm and the software SIMORGH, which is suitable for structural health monitoring (SHM) of civil structures. Initially developed for laboratory-scale hydraulic fracture monitoring, this core software has been effectively scaled up to meter-level applications and is compatible with heterogeneous media such as concrete. It is designed to work with various standard data formats and is handles both trigger-based and continuous data. We present initial results from implementing this software in the AE monitoring of two 4.88-meter-long concrete beams in a laboratory setting, comparing it with manually processed AE data. Our approach enabled the identification of over three times more AE sources than manual processing, achieving higher precision. By processing waveform features in both the time and frequency domains, we successfully classified the damage sources into three categories: tensile, shear, and mixed-mode, at different stages of the experiment. With adequate processing units, the software can operate in parallel, facilitating real-time SHM with exceptional precision in imaging both crack geometry and source types. This involves the incorporation of moment tensor inversion (MTI) to further characterize the physics of AE sources, thereby providing invaluable information to decision-makers regarding the nature of the data captured in real-time.

Keywords: Acoustic Emission monitoring, Moment Tensor Inversion, Structural Health Monitoring, Automation, Real-time monitoring, crack type

Introduction

Fracture nucleation and propagation in solid materials are critical phenomena affecting structural integrity across multiple engineering fields. The prevention of catastrophic failures, such as bridge collapses [1], and the enhancement of processes like geothermal energy extraction by proper hydraulic fracturing [2], are examples of primary areas where understanding these phenomena is vital. Acoustic Emission (AE) monitoring is an established technique for the real-time localization and characterization of active fractures, providing essential data on the evolving geometrical features of these fractures as well as their rupture mechanisms.

The effectiveness of AE monitoring, however, is often hindered by the inherently heterogeneous nature of materials like concrete. This heterogeneity can significantly distort AE signals, necessitating labor-intensive manual signal processing [3]. Moreover, the voluminous data generated, often in the terabyte range, scales linearly with the number of sensors utilized, complicating data management and processing. Consequently, many studies limit sensor numbers to expedite data processing or set higher amplitude thresholds during recording to focus on significant events, potentially omitting critical low-amplitude signals indicative of early-stage fracture development.

The application of moment tensor inversion (MTI), concepts borrowed from seismology, has shown promise for the field of structural health monitoring [4, 5]. These mechanisms provide insights into the orientations and movements along fracture planes during seismic-like events within structures. This information is crucial for predictive maintenance and allows for real-time risk assessment by forecasting the potential impacts of ongoing seismic activities on structures. Furthermore, it assists in rupture characterization of infrastructures and the implementation of early warning systems.

Despite the benefits, currently there is a distinct lack of automated, real-time, scalable solutions for accurate AE monitoring. Recent research studies have explored the integration of deep learning algorithms for source localization of elastic waves [6]. These approaches, while being fast, often require extensive datasets for training neural networks, which do not exist, and achieving the necessary precision and reliability thus remains a challenge.

In conclusion, improving AE monitoring technologies and integrating detailed moment tensor analyses are essential for advancing our understanding of the mechanical behaviors of structures under stress, ultimately enhancing structural safety and operational efficiency across various engineering domains.

In this paper, we present a novel automatic and precise AE source localization and MTI algorithm and software [7, 8, 9]. We show the results of its implementation on reinforced concrete beams that were subjected to cyclic loading and were designed to fail in flexural and shear modes.

1. Laboratory Experiments

1.1 Test specimens and loading protocols

In the Structures Laboratory at the University of Delaware, two large-scale reinforced concrete beams with different shear span ratios and reinforcement configurations were subjected to four-point bending tests. These beams, each with dimensions of 305 mm by 610 mm by 4.88 m (12 in by 24 in by 16 ft), were made of concrete of 31.0 MPa (4,500 psi) and reinforced with Grade 60 steel rebars ($f_y = 414$ MPa). Figure 1a and 1b illustrate the beams under examination.

The first beam, named “flexural beam”, was simply supported over a span of 4.42 m (174 in) and was designed for mid-span flexural failure, incorporated 29 - #3 ($\text{\O} 10$ mm) stirrups, supplemented with 2 - #8 ($\text{\O} 25$ mm) and 4 - #4 ($\text{\O} 13$ mm) longitudinal rebars (see Figure 1a). The beam's flexural capacity, as estimated according to the ACI 318-14 standard, was 340 kNm (251 kip-ft), corresponding to an ultimate applied load of 357 kN (80.2 kip). The second beam, named “shear beam” was simply supported over a span of 3.66 m (144 in) and engineered to fail in shear-mode, as depicted in Figure 1b. This configuration included 22 - #3 ($\text{\O} 10$ mm) stirrups and an equal count of 4 - #8 ($\text{\O} 25$ mm) and 4 - #4 ($\text{\O} 13$ mm) longitudinal rebars. The placement of stirrups was intentionally non-uniform—wider on the right side and narrower on the left side of the mid-span—to induce inclined shear cracks at lower loads without pushing the beam to its failure point. According to ACI 318-14, the shear strength of this beam was calculated at 259 kN (58.2 kips), with a corresponding ultimate load of 518 kN (116 kips). Both beams shared an estimated cracking moment at applied loads of 68 kN (50 kip-ft) and 68.9 kN (15.5 kip), respectively. The two beams were loaded in several load cycles up to failure. More details can be found in [11].

1.2 Recording system and data acquisition

During the experimental testing, Acoustic Emission (AE) signals were captured using a 16-channel high-speed transient recorder (Elsys TraNET FE, Elsys AG, Niederrohrdorf, Switzerland). These signals were recorded for a duration of 1.2 ms at a sampling rate of 10 MHz, initiated when AE activity exceeded a predefined threshold. To optimize detection in areas prone to damage, 15 high-fidelity Glaser/NIST point-contact sensors (KRNBB-PC Sensor, KRN Services, Richland, WA, USA) were placed in a quasi-random around the region of interest. These sensors, which have been absolutely calibrated and found to output a voltage that is proportional to surface displacement [10], were installed in the mid-span and high-shear zones of the beams (illustrated in Figures 1c and 1d), where the formation of flexural and inclined shear cracks were most likely to form. The sensors were mounted using specialized fixtures developed by Mhamdi [11], ensuring precise alignment and constant coupling for effective signal acquisition.

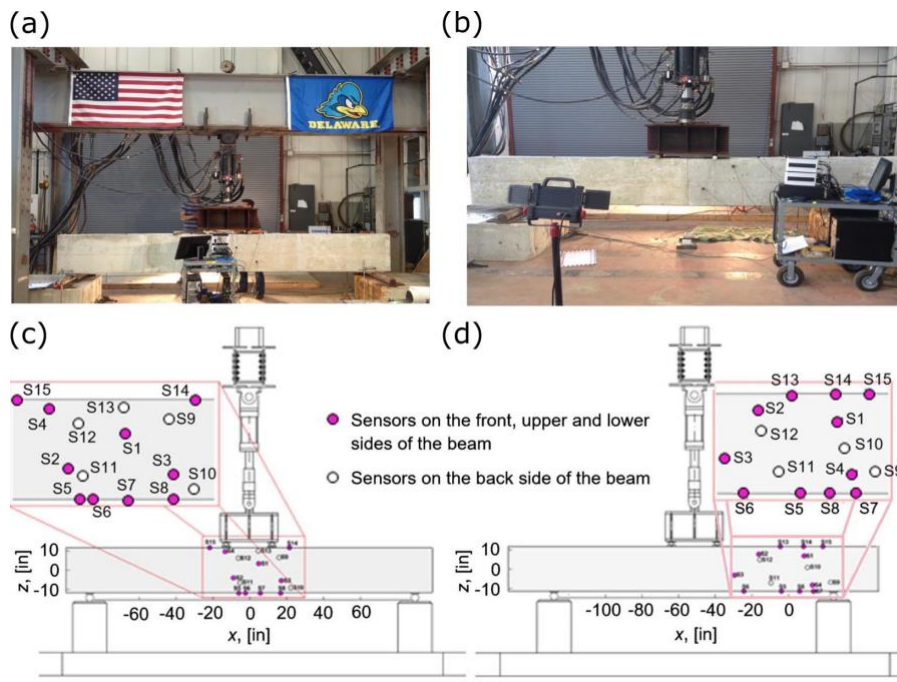


Fig. 1. Experimental test setup with test specimens: (a) Flexural beam and (b) shear beam. Locations of the Glaser/NIST sensors on the (c) flexure beam and (d) shear beam are shown in circles. Full and empty circles denote sensors on the front and back face, respectively. Adapted from [11].

1.3 Flexural beam test

The flexural beam was loaded with three cycles to peak forces of 111 kN (25 kip), 133 kN (30 kip), and 156 kN (35 kip), using a loading rate of 22.2 kN/min (5 kip/min). Each peak load was maintained for several minutes to facilitate thorough inspection for cracks and to document their occurrence before the beam was unloaded at the same rate down to 2.22 kN (0.5 kip). This loading and unloading process was designed to maximize the detection of AE and to accurately document the cracking patterns. AE data were captured and archived following each complete loading cycle. Remarkably, at each loading stage, the SIMORGH software identified over three times more AE events compared to what was originally reported in [11] (see Table 1), which was based on manual processing.

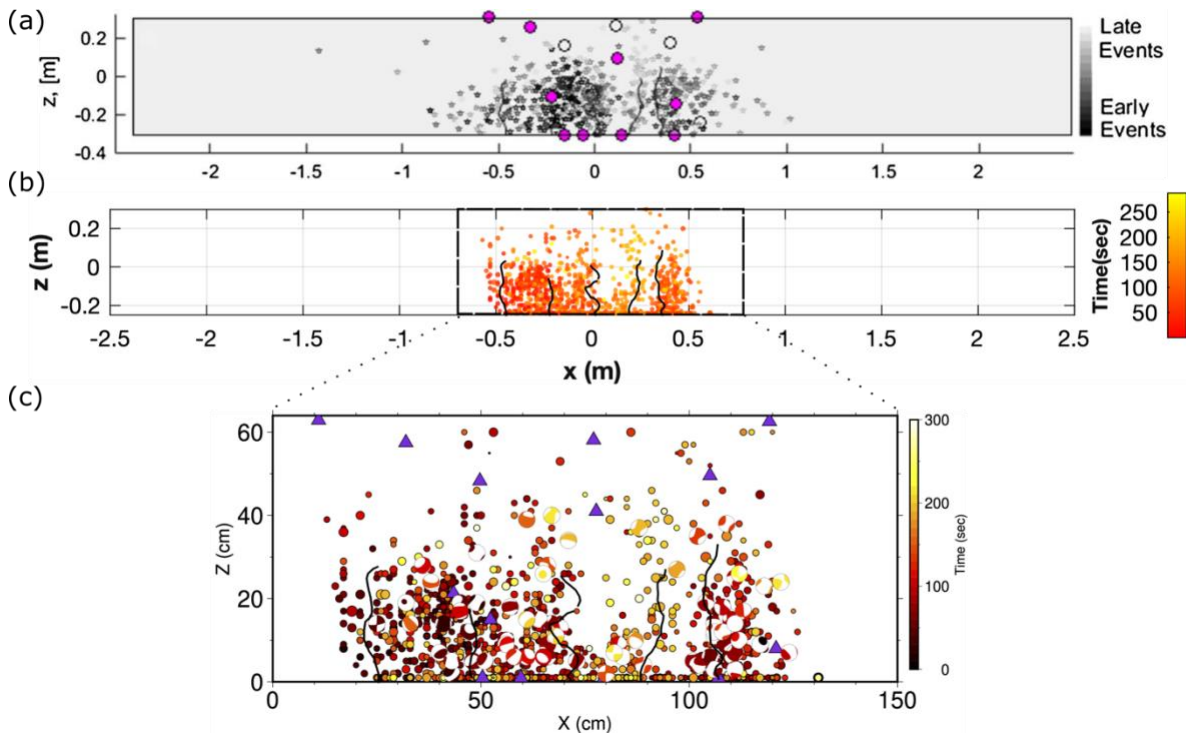


Fig. 2. Sample comparison between 380 AE sources localized by manual processing [(a), Figure from [11] and 1570 AE sources using SIMORGH (b) for the flexural beam loaded to 111 kN (25 kip). Purple circles and triangles show the sensor locations. Curved black lines represent the observed cracks at the end of the experiment. c) 76 moment tensors obtained from the AE showing the fracturing mechanisms.

AE recorded during the first load cycle [111 kN (25 kip)] are presented in Figure 2. The localization errors of these sources were consistent with the findings reported by [11], showing a standard deviation in localizations of maximum 51 mm (2 in).

In the second step of our software pipeline's calculation, the AE that were located by at least eight sensors went through another automated algorithm for MTI calculations, which use body wave polarities and first signal amplitudes. This method is a modified version of [12, 13] that is suitable for heterogeneous media where the Green's functions are not well known for full waveform inversion.

For this load cycle, SIMORGH calculated 460 MTs among which 76 were obtained by at least 8 polarities and their nodal planes were allowed to rotate by maximum of 20° . The moment tensors show consistency with the lineation of AE at different locations (Fig 2c). The Hudson plot shows the clustering behavior of the AE mechanisms being +dipole, -dipole, and mixed mode with shearing components (Fig. 3, left). The Rose diagram shows two main orientations of ruptures having angles of 30° and 60° relative to the applied load (Fig. 3, right).

The distribution pattern of the AEs closely align with the ones reported in [11] and together with the moment tensors, they correlate well with the observed cracking, validating the precision of the AE localizations and source mechanisms calculations by SIMORGH (see Fig. 2).

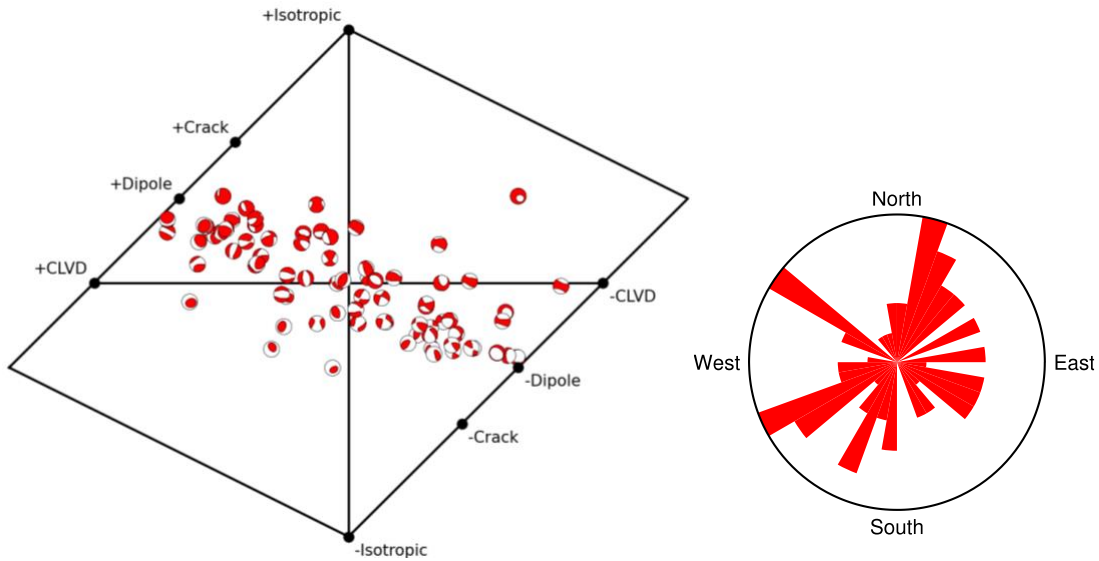


Fig. 3. Left: Hudson plot for the AE moment tensors shown in Figure 2c belonging to the flexural beam loaded to 25 kip. Right: Rose diagram of the moment tensor strikes shown on the left.

Table 1. Comparison of located AE for each load cycle

Test	Loading cycle(kips) min-max	Number of AE (11) Total/selected	Number of AE (SIMORGH) Total/selected	Relative Magnitude range (min/max)
Flexure beam	0-25	674/380	3393/1570	-3.9 / -1.3
Shear beam	0-95	378/207	3050/937	-3.7 / -1.4

1.4 Shear beam test

The shear beam was cyclically loaded from 111 kN (25 kip) to 423 kN (95 kip) in increments of 44.5 kN (10 kip), using the same loading rate used for the flexural beam. The process of holding the load and then unloading was also the same.

Consistent with observations from the flexural beam, SIMORGH demonstrated the capability to detect significantly more AE, up to ten times more [9] in some instances, than manual processing methods described in [11]. The pattern of AE identified by SIMORGH closely resembles the one noted by [11] and aligns with the crack patterns observed in the beam, thereby confirming the accuracy of SIMORGH's AE localization calculations (illustrated in Fig. 4).

Like for the flexural beam, all AE located using at least eight sensors went through the MTI algorithm. In the end, only 25 moment tensors were selected from 49 obtained mechanisms (Fig. 4c). For this set of moment tensors, only one reversed polarity was allowed, and the nodal planes were allowed to move by maximum 25°. These mechanisms together with the AE locations calculated by SIMORGH show an interesting alignment and correlation with the manually localized AE reported in [11] as well as the mapped cracks at the end of the experiment.

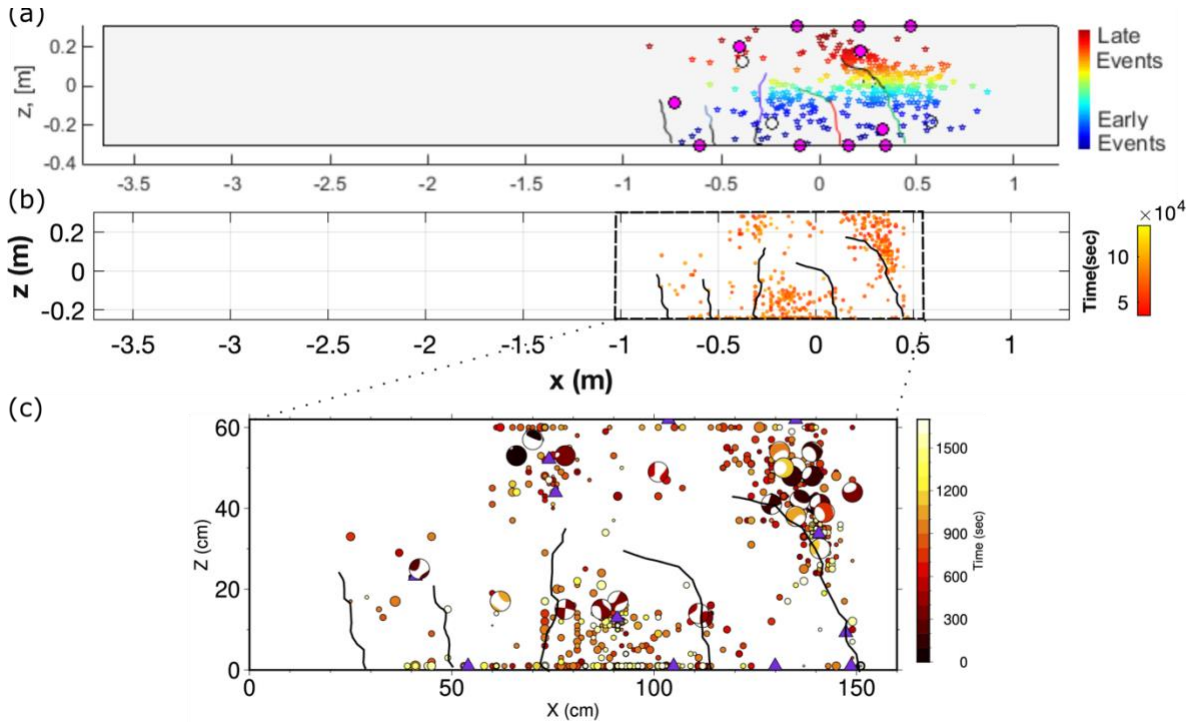


Fig. 4. a, b) Sample comparison between 207 AE sources localized by manual processing [(a), Figure from [11] and 937 AE sources using SIMORGH (b) for the shear beam loaded to 423 kN (95 kip). Purple circles and triangles show the sensor locations. Curved lines show the observed cracks at the end of the experiment. c) 25 selected moment tensors from the AE show the fracturing mechanisms.

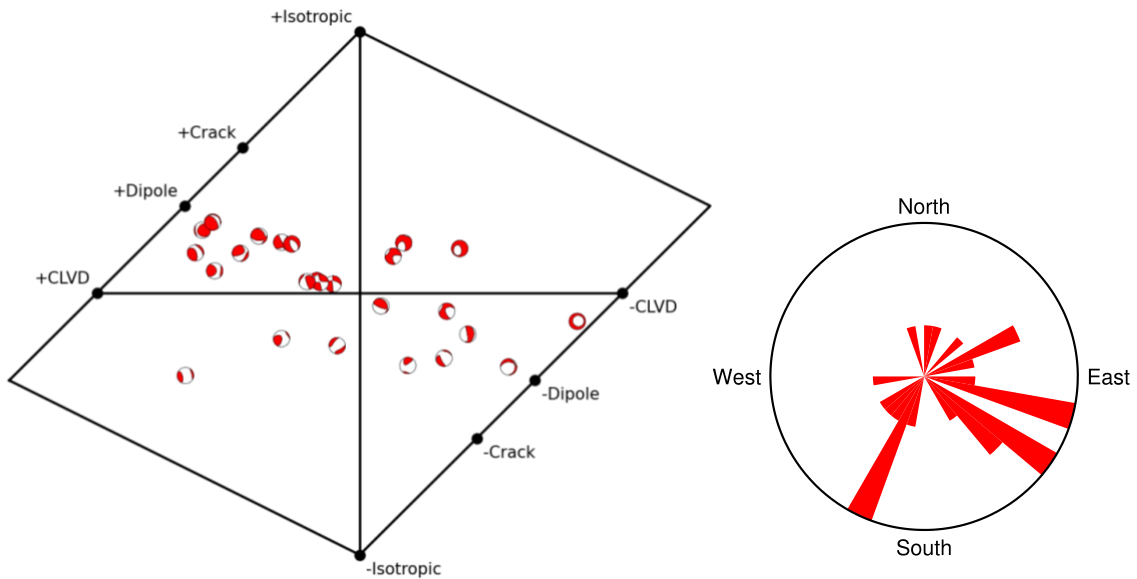


Fig. 5. Left: Hudson plot for the AE mechanisms shown in Figure 4c belonging to the shear beam from the last loading stage, 423 kN (95 kip). Right: Rose diagram of the moment tensor strikes shown on the left.

Figure 5 shows the Hudson plot of the 25 moment tensors indicating their main mechanism being shear with some others close to +dipole. Their Rose diagram shows the three main strikes having angles of 20° to 40° and 60° with the vertical load. The change in orientation is correlated with the bending of the fracture having mixed-mode mechanisms of shearing and opening. Some of the MTs are not aligned with the last stage of AE distribution as well as the final observed crack geometry, and most likely belong to previous loading stages.

2. Discussion

Proper signal processing, accurate application of the medium velocity model during calculations, and the selection of an appropriate calculation method are essential for the precise localization of AE sources. Manual localization of a single AE source generally takes 2 to 3 minutes, influenced by factors such as the number of sensors (typically between eight and 20) and the signal quality required to determine the arrival times of the P and S waves. Calculating the source mechanism using MTI typically requires more time than localizing sources and is usually performed during the post-processing stage. However, SIMORGH can localize an AE source and calculate its moment tensor in less than a second. This efficiency is achieved by utilizing every available processor within the computing unit, allowing for a parallelized approach that supports real-time, detailed fracture monitoring with high precision, assuming sufficient computational power is available.

SIMORGH is adept at navigating all potential medium complexities, from homogeneous to fully 3D velocity models, employing the Eikonal equation to determine the shortest ray path. It assesses each potential path before selecting the most probable solution. Users have the flexibility to modify over 50 defined hyper-parameters to refine calculations. A significant recent enhancement to the software is the automatic MTI, which elucidates the fracturing mechanism of the material, adding another layer of depth to the analysis. SIMORGH provides detailed information about each AE source's mechanism in real-time. These source mechanisms undergo validation through various standard methods, including station removal, the Jackknife test, and the examination of potential reversed polarities due to medium heterogeneity.

When processing AE data from the two concrete beam tests described, SIMORGH demonstrated its capability to compute results approximately 1000 times faster than the manual methods referenced in [11]. It identified three to ten times more AE that met similar precision criteria. The moment tensors reveal a range of mechanisms, from positive dipole and negative dipole to mixed modes of opening-closing with shearing components. These mechanisms align with the localized AEs, highlighting the consistency between the two sets of results.

For the flexure test, we have obtained more MTs demonstrating opening-closing crack mechanisms (distributed toward both positive and negative dipoles on the Hudson plot in Fig. 3) compared to the shear test. As expected, cracking with a compressional mechanism is mainly observed close to the load points at the top of the beams in both experiments. For the flexure test, opening crack mechanisms are more commonly observed at the bottom of the beam, particularly toward the end of the experiment. MTs exhibiting a mixed mode of opening and shearing are very common, which is a result of river-shaped fracturing.

For the shear test, we observe patterns of acoustic emissions (AEs) distribution similar to the cracks observed at the end of the experiment. The moment tensors (MTs) exhibit a wide variety of mechanisms, which is expected since this is the last load cycle of the experiment and several fractures with complex geometries have already been created. MTs with opening mechanisms are primarily obtained on the right side of the shear beam test where the fracture is bent. This is indeed because these results are from the last loading cycle of the beam, and the predominant mechanisms in that location, at that time, are opening.

The Rose diagrams of MT strikes indicate two main orientations roughly at angles of 30° and 60° relative to the loading vectors for both flexure and shear tests. However, a slight divergence at the angles of 20° and 40° in the Rose diagram for the shear test may be an indicator of the bent crack. A comprehensive interpretation of results from all loading cycles is necessary to better understand the differences between the two tests.

3. Conclusion

SIMORGH significantly increases efficiency by reducing the time and costs associated with processing localization and source mechanism calculation tasks, without compromising precision. This enhancement enables real-time monitoring, which is a vital requirement across various industries but is not currently feasible. Industries that benefit from such capabilities include those involved with monitoring fracture development in tailing dams and dam structures, geothermal energy production, Carbon Capture and Storage (CCS), and the mining, oil, and gas sectors. Additionally, real-time monitoring is crucial for landslide-prone areas, as well as the maintenance and safety of aircraft, railways, and other critical infrastructures.

The implementation of SIMORGH enables the confident and cost-effective deployment of Acoustic Emission/Microseismic (AE/MS) surveillance arrays. As a result, these arrays can be more widely and routinely installed, enhancing public safety. In summary, the development of this software is poised to have a profound impact on community security, safety, and environmental sustainability.

Acknowledgement

This work is supported by the Swiss National Science Foundation (SNSF), Bridge Proof of Concept grant numbers: 40B1-0_214632 and 40B1-0_214632 - 2.

References

- [1] https://en.wikipedia.org/wiki/List_of_bridge_failures
- [2] Park, S., K.I. Kim, L. Xie, et al. 2020. "Observations and analyses of the first two hydraulic stimulations in the Pohang geothermal development site, South Korea" *Geothermics*, 88, 101905, <https://doi.org/10.1016/j.geothermics.2020.101905>.
- [3] Li, L., J. Tan, B. Schwarz, F. Staněk, N. Poiata, P. Shi, et al. 2020. "Recent advances and challenges of waveform-based seismic location methods at multiple scales" *Reviews of Geophysics*, 58, e2019RG000667. <https://doi.org/10.1029/2019RG000667>.
- [4] Linzer, L., Mhamdi, L., and Schumacher, T. (2015). "Application of a moment tensor inversion code developed for mining-induced seismicity to fracture monitoring of civil engineering materials." *J. Appl. Geophys.*, 112, 256–267.
- [5] Grosse, C.U., Ohtsu, M., 2008. *Acoustic Emission Testing*. Springer Science & Business Media.
- [6] Van den Ende M.P.A., and J.P. Ampuero. 2020. "Automated seismic source characterization using deep graph neural networks" *Geophysical Research Letters*, 47(17), doi:10.1029/2020GL088690
- [7] Momeni, S., D. Liu, and B. Lecampion. 2021. "Combining active and passive acoustic methods to image hydraulic fracture growth in laboratory experiments". *Eurock21*, Turin, Italy, DOI:10.1088/1755-1315/833/1/012088.
- [8] Momeni, S., G. Lu, and B. Lecampion, 2021. "Automatic passive acoustic emission-microseismic monitoring using a parallel algorithm; A case study of a hydraulic-fracturing experiment" *SGM 19*, Geneva, Switzerland.
- [9] Momeni, S., T. Schumacher, L. Linzer, B. Lecampion, 2023. "Automatic and high-precision acoustic emission-based structural health monitoring of concrete structures" *IWSHM2023*, Stanford, CA, USA.
- [10] Mclasley, G.C., Glaser, S.D. (2013). Absolute Calibration of an Acoustic Emission Sensor. In: Güneş, O., Akkaya, Y. (eds) *Nondestructive Testing of Materials and Structures*. RILEM Bookseries, vol 6. Springer, Dordrecht. https://doi.org/10.1007/978-94-007-0723-8_9
- [11] Mhamdi, L. 2015. "Seismology-based approaches for the quantitative acoustic emission monitoring of concrete structures." *Ph.D. dissertation, Univ. of Delaware*, Newark, DE.
- [12] Fitch, T. J., D. W. McCowan, and M. W. Shields (1980). Estimation of seismic moment tensor from teleseismic body wave data with application to intraplate and mantle earthquakes, *J. Geophys. Res.* 85, 3817–3828.
- [13] Andersen, L. M. (2001). *A Relative Moment Tensor Inversion Technique Applied to Seismicity Induced by Mining*, Univ. of the Witwatersrand, Johannesburg.